Published in final edited form as:
ACS Sustain Chem Eng. 2013 July 1; 1(7): 833–842. doi:10.1021/sc400042h.

Adsorption of a Protein Monolayer via Hydrophobic Interactions Prevents Nanoparticle Aggregation under Harsh Environmental Conditions

Sergio Dominguez-Medina[1], **Jan Blankenburg**[1], **Jana Olson**[1], **Christy F. Landes**[1,*], and **Stephan Link**[1,2,*]

[1]Department of Chemistry, Laboratory for Nanophotonics, Rice University, Houston, Texas 77005

[2]Department of Electrical and Computer Engineering, Laboratory for Nanophotonics, Rice University, Houston, Texas 77005

Abstract

We find that citrate-stabilized gold nanoparticles aggregate and precipitate in saline solutions below the NaCl concentration of many bodily fluids and blood plasma. Our experiments indicate that this is due to complexation of the citrate anions with Na^+ cations in solution. A dramatically enhanced colloidal stability is achieved when bovine serum albumin is adsorbed to the gold nanoparticle surface, completely preventing nanoparticle aggregation under harsh environmental conditions where the NaCl concentration is well beyond the isotonic point. Furthermore, we explore the mechanism of the formation of this albumin 'corona' and find that monolayer protein adsorption is most likely ruled by hydrophobic interactions. As for many nanotechnology-based biomedical and environmental applications, particle aggregation and sedimentation are undesirable and could substantially increase the risk of toxicological side-effects, the formation of the BSA corona presented here provides a low-cost bio-compatible strategy for nanoparticle stabilization and transport in highly ionic environments.

Keywords

Gold nanoparticles; surface plasmon; bovine serum albumin; protein corona; correlation spectroscopy; diffusion

Introduction

Human blood plasma, the liquid part of blood, is a complex environment with thousands of proteins, antigens and antibodies diffusing in a solution with relatively high ionic strength (NaCl concentration of ~ 150 mM).[1,2] Nanoparticles are currently investigated for their clinical use in disease diagnosis and treatment.[3–7] Any practical application of nanoparticles in biological fluids, such as blood plasma, should ensure monodispersity of the material under these harsh conditions, as particle agglomeration and sedimentation[8,9] may affect the biodistribution of the material and lead to harmful side effects.[10,11]

*Corresponding authors, cflandes@rice.eduslink@rice.edu.

Supporting Information Available

Size distributions of 51 nm AuNPs obtained using TEM images, Ellman's reagent assay for thiol activity of BSA and SB-BSA along with positive and negative controls, autocorrelation traces of 50 nm AuNPs and 110 nm latex beads used as calibration standard for correlation spectroscopy experiments, characteristic diffusion times and hydrodynamic dimensions of 50 nm AuNPs and 110 nm latex beads, UV/Vis ensemble extinction measurements of AuNPs in $ZnCl_2$ and $CaCl_2$, and BSA-coated AuNPs in NaCl, PBS and TBS. This material is available free of charge via the Internet at http://pubs.acs.org

Alongside the issue of particle dispersity, exposure of nanoparticles to blood leads to adsorption of plasma proteins onto their surface,[12–17] affecting how cellular receptors screen nanomaterials.[18–23] While studies characterizing this protein 'corona' are rising, quantitative investigations of how this corona may affect the dispersity and mobility of nanoparticles are still scarce.[9,11,24] In addition, the role of the ionic strength of biological fluids in the affinity between proteins and nanoparticles is a fundamental aspect that needs further investigations.[25–28]

Serum albumin, the most abundant protein in circulation, will likely play a key role in the transport of nanoparticles across the bloodstream, as its main biological function is the transport of non-polar compounds in the circulatory system.[29,30] Bovine serum albumin (BSA) often serves a model protein for nanoparticle-protein studies, as it shares 98 % of its aminoacid sequence with its human variant.[29] Although this protein is negatively charged at physiological pH, it also contains eleven hydrophobic binding domains, 66 positively charged lysines and an unpaired sulfhydryl group (cysteine).[30] Given the complexity of this protein, its interaction with nanoparticles is by no means trivial.

Gold nanoparticles (AuNPs) are ideal candidates for fundamental studies of protein-nanoparticle interactions. [13,31–33] Upon interaction with light, high absorption and scattering cross sections across the visible and near IR spectral region arise from the collective oscillation of the conduction electrons, a phenomenon known as the surface plasmon resonance.[34–37] The field of plasmonics[38] has promising applications in biology and medicine such as high contrast nanoparticle imaging, tracking, and sensing.[39–44] In addition, recent *in vivo* studies have found low-toxicity associated with the gold core for nanoparticle sizes around 50 nm in diameter.[7,10,45] While many ligand-exchange strategies have been realized for AuNPs,[46–52] citrate stabilization via electrostatic repulsion is still the simplest low-cost route for particle synthesis that does not require covalent attachment of molecules to the surface.[53–56]

The interaction of citrate-stabilized AuNPs and bovine and human serum albumin has been reported in the literature and is now extensive.[31,32,57–63] The proposed mechanisms to explain this interaction can be grouped into two categories: 1) Electrostatic attraction between the positively charged lysine groups of the protein and the citrate-layer covering the gold surface;[31,57,60,62] 2) Thiol-binding of the cysteine residues, in particular cys-34, directly to the gold surface, most likely displacing the citrate layer on the gold surface.[59,61]

Here we show that aqueous solutions with the same pH and ionic strength as human blood plasma cause aggregation and precipitation of citrate-stabilized AuNPs. Our experiments suggest that this occurs due to complexation of the citrate molecules with counter ions in solution. Adsorption of BSA onto the nanoparticle surface enhances the colloidal stability at salt concentrations beyond the isotonic point (> 100 mM), a positive side effect of the BSA protein-corona. Additionally, we address the ongoing debate of the binding mechanism of BSA on citrate-stabilized AuNPs by testing the adsorption of the protein under different saline conditions and with a sulfhydryl-blocked form of BSA. Finally, we demonstrate that the ionic strength of the solution drives the adsorption of BSA to AuNPs, as the binding affinity increases in the presence of salts due to an overall increase of the nanoparticle hydrophobicity.

Experimental Section

Materials

Citrate-stabilized AuNPs with a nominal diameter of 50 nm and an approximate concentration of 10^{10} AuNPs/mL were purchased from BBInternational. The sample was

further characterized by transmission electron microscopy (TEM, JEOL 2010), yielding an average diameter of 51 ± 7 nm. A representative TEM image is shown in Figure S1, along with the size distribution obtained using a home-built image analysis program written in Matlab.

NaCl, $CaCl_2$, and $ZnCl_2$ were purchased from Sigma-Aldrich. Solutions of these salts were prepared in Milli DI water (> 25 MΩ, Millipore). The behavior of AuNPs in saline solutions was studied by mixing equal volumes of citrate-stabilized AuNPs and salt solutions. The salt concentration reported throughout the manuscript is the final concentration after mixing with AuNPs. Phosphate buffered saline (PBS) and Tris-buffered saline (TBS, NaCl = 150 mM) were purchased from Sigma-Aldrich. The pH of all saline solutions was measured and found to be in the in the physiological range (7.0 – 7.5).

Albumin from Bovine Serum was purchased from Sigma-Aldrich (≥98 % lyophilized powder, product number A7906, M_W = 66430). Sulfhydryl-blocked Bovine Serum Albumin (SB-BSA) was purchased from Lee Biosolutions (≥ 98 % lyophilized powder, product number 100-10SB, M_W = 66317). The purity of these BSA samples is comparable to other studies of nanoparticle-protein interactions.[31,32,57,59] The proteins were diluted to the desired concentration in molecular biology grade water at the required salt concentration. To prevent protein aggregation, protein solutions were freshly prepared for each experiment. The BSA lyophilized powder was stored at 2 °C. For protein binding experiments, AuNPs and BSA were mixed using equal volumes of each solution. The protein concentration reported throughout the manuscript is the final concentration after mixing.

Ellman's reagent (5,5′-dithiobis-(2-nitrobenzoic acid), Sigma Aldrich) was used to quantify the thiol activity of BSA and SB-BSA using UV/Vis spectroscopy.[64] Figure S2A shows the UV/Vis extinction of Ellman's reagent after reacting with BSA and SB-BSA, as well as with positive (thiol-PEG, Sigma Aldrich) and negative controls (H_2O, Millipore). The lack of thiol activity of SB-BSA is confirmed by its weak absorbance at 412 nm (Figure S2B) when compared to the sample with just water.

Microscope cover glass slides (25 × 25 mm^2, Fisherbrand) were sonicated in acetone (ACS spectrophotometric grade, Sigma-Aldrich) and Milli Di water for 20 min. The slides were then dried with ultra-high purity N_2 (Matheson) and stored in SampleStorr™ vacuum containers (Ted Pella, Inc) to avoid contamination. Before use, the microscope slides were cleaned with O_2 plasma for 90 s at 200 mTorr (Harrick Plasma). Silicon chambers (50 μL, Grace Bio-Laboratories) were placed on top of the microscope cover glass and filled with the solution of interest using a micropipette (Thermo Scientific).

UV/Vis spectroscopy and Zeta-potential measurements

Ensemble UV/vis spectroscopy of the AuNPs solutions was measured using a home-built optical setup with a fiber spectrometer from Ocean Optics (SD1024DW). A cuvette containing approximately 1 mL of solution was illuminated using a white LED light source (MWWHL3, Thorlabs). The incident power was adjusted with a 15 V power supply unit and a LED driver (Thorlabs) to avoid saturation of the detector. The experiment was controlled using the SpectraSuite spectroscopy software supplied by Ocean Optics. Zeta-potential values were acquired using a Malvern Zen 3600 (Zetasizer Nano). The Smoluchowski approximation was used as an input parameter of the Henry equation, corresponding to the electrophoretic mobility of small particles in aqueous media.

Scattering correlation spectroscopy

Scattering correlation spectroscopy was performed using a home-built inverted microscope (Observer.D1, Zeiss) described elsewhere.[65] Light from a 532 nm laser (Verdi-6, Coherent

Inc.) was circularly polarized using a λ/4 wave plate, then collimated and expanded to overfill the objective (Fluar, Zeiss: 100 X, NA = 1.3). The laser power was attenuated using neutral density filters (Thorlabs) to approximately ~ 400 nW, measured before the microscope. Heating of the sample in this power range is negligible.[65] The focal plane of the objective was set to approximately ~ 6 μm inside the sample, to avoid excessive scattered light from the glass-water interface. The scattered light was collected in the backwards direction, and redirected to a 50 μm pinhole before focusing into an avalanche photodetector (SPCM-AQRH, Perkin Elmer). To ensure that only elastic scattering is collected, a 532 ± 2 nm band pass filter was placed in the detection beam path.

Scattering correlation spectroscopy is a photon correlation technique that measures the Brownian fluctuations in the scattering intensity caused by particles diffusing through a diffraction limited focal volume. Because the analyte concentration is typically below the nanomolar regime, it is assumed here that only one particle is diffusing through the focal volume at a time. The temporal autocorrelation $G(\tau)$ of the scattering signal $I(t)$ was performed over a range of lag times from τ_{min} to τ_{max} as:

$$G(\tau)=\frac{\langle \delta I(t)\delta I(t+\tau)\rangle}{\langle \delta I(t)\rangle^2} \quad (1)$$

where $\delta I(t)$ represents an intensity fluctuation, mathematically expressed as the intensity at time t minus the average: $\delta I(t) = I(t) - \langle I(t)\rangle$. For the ideal case of three-dimensional Gaussian excitation in a confocal microscope, the autocorrelation function can be expressed in terms of the average number of species crossing the focal volume $\langle N\rangle$, the beam waist r_0, and beam height z_0:66

$$G(\tau)=\frac{1}{\langle N\rangle}\frac{1}{\left(1+\frac{\tau}{\tau_D}\right)}\frac{1}{\left(1+\left(\frac{r_0}{z_0}\right)^2\left(\frac{\tau}{\tau_D}\right)\right)^{1/2}} \quad (2)$$

The characteristic diffusion time τ_D and the geometrical factor $\left(\frac{r_0}{z_0}\right)$ are used as fit parameters in equation (2). The amplitude of the autocorrelation function $\frac{1}{\langle N\rangle}$ is normalized to 1 for better comparison of the differences in τ_D under different salt and protein concentrations. After extracting τ_D from at least 3 independent measurements of 7 intensity transients (40 s each), the translational diffusion coefficient D_{tr} was calculated according to:

$$\tau_D=\frac{r_0^2}{4D_{tr}} \quad (3)$$

D_{tr} is related to the hydrodynamic radius R_h using the Stokes-Einstein relationship:

$$D_{tr}=\frac{kT}{6\pi\eta R_h} \quad (4)$$

where k is the Boltzmann constant, T is the temperature (T = 296 ± 1 K), and η is the solvent viscosity. For H_2O at room temperature we used η = 0.89 mPa·s. While the effect of the salts (NaCl, $ZnCl_2$, and $CaCl_2$) on the viscosity of the aqueous solutions is negligible for the range of concentrations tested, the effect of BSA was considered using a linear

approximation based on the intrinsic viscosity of the protein according to the provider, $[\eta] = 4.13\ cm^3\ g^{-1}$. This same approximation was used for SB-BSA.

Following previously published criteria for consistent correlation spectroscopy analysis,[67] the minimum and maximum lag times were set to $\tau_{min} = 10\ \mu s$ and $\tau_{max} = 40\ s$. The dimensions of the focal volume are obtained using 110 nm latex beads purchased from Invitrogen (C37485). Figure S3 shows the autocorrelation function of 110 nm latex beads which were used as a standard to extract the hydrodynamic dimensions of the AuNPs (Table S1).

Results and Discussion

Citrate-stabilized AuNPs precipitate in NaCl solutions at physiological pH. Figure 1A shows the extinction spectra of AuNP solutions for different NaCl concentrations. The spectra were acquired after 24 hours of equilibration. The extinction of the surface plasmon resonance at its maximum $\lambda_{max} = 535$ nm decreases with increasing NaCl concentration. To better understand the underlying mechanism of AuNP precipitation, spectra were also acquired as a function of time after initial mixing as shown in the inset of Figure 1A.

While the spectra at equilibrium show that AuNPs precipitate out of solution in the presence of NaCl, the spectral acquisition as a function of time after initial mixing strongly indicates particle aggregation in the early stages of precipitation, observed as a red-shift and broadening of the plasmon band. The time dependent spectra were acquired at a higher NaCl concentration of 100 mM for a faster visualization of this process. It should be noted however that the lower concentrations of NaCl shown in the main panel induce similar aggregation and precipitation but on longer time scales (data not shown). The red-shift of the plasmon peak occurs as a result of plasmon coupling within AuNP aggregates,[37] but as time increases this red-shifted band vanishes as the aggregates fall out of solution.

The decrease in the extinction of the plasmon resonance occurs together with an increase in the AuNPs zeta-potential. Figure 1B shows the extinction at λ_{max} extracted from Figure 1A, alongside with zeta-potential measurements of the AuNP colloids also acquired at equilibrium. The zeta-potential increases with increasing NaCl concentration. Note that at NaCl concentrations higher than 15 mM the error bars substantially increase as the solution concentration decreases. Pictures of the AuNPs solutions are also shown in Figure 1B. Whereas at 1 mM NaCl the solution is bright red due to the plasmon resonance of the colloidal AuNPs, the solution turns clear at 30 mM because the AuNPs have formed aggregates and precipitated.

Two hypotheses can be formulated to explain the increase in zeta-potential shown Figure 1B: 1) The formation of an electric double layer of Na^+ cations binding to the citrate, or 2) complexation of the citrate anions with counter ions in solution, as it is well known that citrate can form complexes with metallic salts in aqueous environments.[68] To gain more insight into the salt-triggered aggregation mechanism, extinction spectra of the same citrate-stabilized AuNPs were acquired in $CaCl_2$ and $ZnCl_2$ solutions (Figure S4), thereby changing the cations but keeping the same amount of net charge for these two conditions(Ca^{2+}, Zn^{2+}). As seen in Figure S1A, as little as 80 μM of $CaCl_2$ can precipitate the colloid almost entirely. $ZnCl_2$, on the other hand, requires a concentration of at least an order of magnitude higher (~ 800 μM) in order to achieve complete precipitation.

Because Ca^{2+} and Zn^{2+} have the same net charge, the dramatically different concentrations required for nanoparticle precipitation does not support the formation of an electric double layer. The experiments with NaCl shown in Figure 1 do not support this hypothesis either because 30 mM NaCl was required to induce colloid precipitation, an order of magnitude

higher concentration than for Ca^{2+}, despite having only half the charge. If an electric double layer were formed, the amount of salts required to crash the nanoparticles would not differ by an order of magnitude between the salts tested. The order of the complexation (Ca^{2+}> Zn^{2+} > Na^{+}) also agrees well with the reported complexation affinity of citrate with these metal ions.[68] We therefore conclude that nanoparticle aggregation and subsequent precipitation likely occur because the citrate anions form complexes with counter cations in solution. This process removes the citrate layer, thereby exposing the bare, unprotected nanoparticle surface.

Further support of the formation of nanoparticle aggregates in the presence of NaCl is observed via scattering correlation spectroscopy. Because of the diffraction limited detection volume, and the scaling of the scattering intensity with V^2,[36] scattering correlation spectroscopy is a powerful technique for the detection of small amounts of aggregates in heterogeneous samples. In our previous work we observed that as small as a 2% contamination of a colloid with larger nanoparticles dramatically bias the autocorrelation curves to longer diffusion times.[65] Figure 2A shows the autocorrelation traces of AuNPs before and after addition of 40 mM NaCl approximately 10 min after preparation. Note that from the data in Figure 1A, this NaCl concentration can precipitate the colloid entirely in about a day. The increase of one order of magnitude in the characteristic diffusion time τ_D from ~ 1 ms to ~ 10 ms implies a similar increase in the hydrodynamic radius R_h from 26 nm to ~ 250 nm, resulting from particle aggregation. Therefore, Figure 2A demonstrates that large and slow aggregates are diffusing through the observation volume in the presence of NaCl.

The raw intensity traces used in the autocorrelation analysis also contain useful information for the detection of particle aggregates. Figure 2B shows a blip intensity frequency analysis (BIFA) of the same autocorrelation traces shown in Figure 2A. BIFA plots the frequency and intensity (photon counts) of scattering events for a fixed amount of time for an intensity vs. time trace (40 s in this case as shown in the inset of Figure 2B). The formation of aggregates not only shifts the intensity histograms toward larger values, but also decreases the number of events detected per time interval. Fewer but brighter events are a result of larger particle aggregates formed in solution. Having discussed the salt-induced aggregation and precipitation of citrate-stabilized AuNPs, we now explore the effect of BSA adsorption on the stability and diffusion of AuNPs in saline solutions.

Addition of BSA to the AuNPs in the range of physiological concentrations ([BSA] = 375 μM), *before* mixing with NaCl stabilizes the colloid even at concentrations beyond the isotonic point ([NaCl] > 100 mM). Figure 3A shows the extinction spectra of AuNP solutions with increasing NaCl concentrations, measured after 24 hours of preparation. The AuNPs were stable even at similar NaCl concentrations to that found in seawater (~ 1000 mM), and in commonly used buffer solutions such as phosphate buffered saline (PBS) and tris buffered saline (TBS) (Figure S5). In contrast to the salt-dependent precipitation observed in Figure 1, the AuNPs remain stable in the presence of large amounts of NaCl.

This enhanced colloidal stability in environments with high ionic strength is observed even if BSA and NaCl are *simultaneously* added to the citrate-stabilized AuNPs. The inset of Figure 3A shows extinction spectra acquired immediately after simultaneous addition of 375 μM of BSA and 100 mM of NaCl (t = 0 s, solid cyan line), and ten min later (t = 600 s, dashed red line). The extinction spectrum remains completely unchanged, strongly suggesting that particle stabilization via protein adsorption occurs at a faster time scale than particle aggregation and precipitation.

Adsorption of BSA onto citrate-stabilized AuNPs increases the nanoparticle zeta-potential. Figure 3B shows the extinction at λ_{max} of the same spectra shown in Figure 3A, alongside with zeta-potential measurements of the same AuNP solutions. The offset in the zeta-potential observed at 0 mM NaCl (− 30 mV) in the presence of BSA, in comparison to the zeta potential in the absence of BSA (− 50 mV, Figure 1B) is strong evidence of protein adsorption.[31,60] Although the intensity and shape of the extinction spectra remain unaffected in a wide range of NaCl concentrations, the nanoparticle zeta-potential increases as the NaCl concentration increases. The fact that the zeta-potential increases toward neutral values as the NaCl concentration increases could imply that more BSA is bound to the nanoparticle surface, as this protein is just slightly negatively charged at physiological pH. As the protein concentration is kept constant at 375 μM, this conclusion is not obvious and would imply that the salt concentration drives the affinity between BSA and AuNPs, as will be discussed in more detail below.

Further support of the enhanced colloidal stability provided by BSA in saline solutions is shown via scattering correlation spectroscopy. Figure 4A shows the autocorrelation curve of the original citrate-stabilized AuNP solutions (0 mM NaCl + 0 mM BSA, blue squares). Addition of BSA at concentrations in the physiological range (375 μM) increases the characteristic diffusion time τ_D, corresponding to an increase in the nanoparticle hydrodynamic radius from $R_h = 26 \pm 2$ nm (blue squares) to $R_h = 31 \pm 2$ nm (black squares), in agreement with our previously published results of BSA monolayer adsorption onto citrate-stabilized AuNPs.[69] The observed change in hydrodynamic radius after addition of BSA to the AuNPs corresponds to the formation of a BSA monolayer on the citrate-stabilized AuNPs, based on the dimensions of the native form of the protein.[29] Addition of 40 mM NaCl to this BSA-AuNP system yields identical autocorrelation traces (red squares).

In agreement with Figure 4A, BIFA (Figure 4B) shows almost identical intensity histograms for BSA-stabilized (375 μM) AuNPs in 0 mM (black) and 40 mM (red) NaCl solutions. In addition, the number of events counted for a time interval of 40 s remains similar for both solutions. Scattering correlation spectroscopy and BIFA therefore demonstrate that AuNP diffusion is unaffected by the NaCl concentration of the solution and that the nanoparticles do not aggregate once BSA is adsorbed onto the AuNP surface.

Addition of BSA *after* adding NaCl immediately stops the salt-induced aggregation. Figure 5A shows UV/Vis extinction spectra of citrate-stabilized AuNPs for the first 600 s after mixing with 100 mM NaCl. This NaCl concentration was chosen to speed-up the salt-induced precipitation before BSA addition. Following a similar trend as observed in the inset of Figure 1A, the AuNP colloid starts to aggregate and precipitate quickly. Addition of 50 μM BSA after 10 s immediately stops the precipitation process, as the extinction spectra of the AuNPs are all identical after BSA has been added to the solution. This particular BSA concentration was selected to reduce the effect of the protein's viscosity in the mixing with AuNPs, but larger BSA concentrations are expected to produce the same enhanced stability. BSA adsorption must therefore occur on a faster time-scale than the NaCl induced aggregation and citrate-complexation, however further experiments would be necessary to quantitatively measure the competitive kinetics between these two processes.

Having discussed the enhanced stability provided by BSA to AuNPs in environments that would otherwise induce aggregation, we now explore the question of the physico-chemical mechanism for BSA adsorption on AuNPs. As stated in the introduction, some studies have proposed that BSA binds to AuNPs using the unpaired sulfhydryl group of cysteine-34, forming a thiol bond with the gold surface. If this is the case, a sulfhydryl-blocked form of BSA (SB-BSA) should not adsorb onto the AuNP surface and hence not provide the enhanced colloidal stability in environments with high ionic strength as native BSA does.

The sulfhydryl-blocked form of BSA provides the same enhanced colloidal stability as native BSA in salt solutions. In a similar manner as Figure 5A, Figure 5B shows UV/Vis extinction spectra of AuNPs in 100 mM NaCl as a function of time for the first 600 s after adding salt. The salt-induced precipitation is stopped after 10 s by addition of 50 μM SB-BSA, as evidenced by the identical extinction spectra observed for the remaining 590 s of spectra acquisition. To further verify that the enhanced colloidal stability provided by SB-BSA comes from adsorption onto the AuNPs surface, scattering correlation spectroscopy experiments were performed.

BSA and SB-BSA are both adsorbed on citrate-stabilized AuNPs. Scattering correlation spectroscopy experiments demonstrate that in the presence of physiological concentrations of BSA (Figure 6A) and SB-BSA (Figure 6B), the autocorrelation curves shifts to slower characteristic diffusion times as a result of protein adsorption onto the nanoparticle surface. The calculated hydrodynamic radius of citrate-stabilized AuNPs grows from $R_h = 26 \pm 2$ nm to $R_h = 31 \pm 2$ nm in BSA and $R_h = 30 \pm 2$ nm in SB-BSA. These changes in hydrodynamic radii correspond to no more than monolayer adsorption of both forms of BSA onto citrate-stabilized AuNPs. These results strongly suggest that the dominant mechanism for adsorption is not via the unpaired-thiol group of BSA.

So far we have established that salts in solution assist the complexation of citrate anions with salt-cations (such as Na^+, Ca^{2+} or Zn^{2+}), leaving the AuNP surface with little electrostatic protection for effective particle-particle repulsion. We also found that BSA binding onto the AuNP surface occurs faster than the citrate-complexation induced precipitation of the colloid. Because the enhanced colloidal stability comes from BSA-adsorption, we therefore further hypothesize that the presence of salts must have an effect on the binding affinity between BSA and citrate-stabilized AuNPs. To explore this in detail, BSA adsorption isotherms at two distinct NaCl concentrations were obtained using scattering correlation spectroscopy.

The binding affinity of BSA to AuNPs increases in the presence of NaCl. Figure 7 shows the AuNP hydrodynamic radius, extracted from scattering correlation spectroscopy analysis (blue squares), as a function of BSA concentration for 0 mM (Figure 7A) and 20 mM NaCl solutions (Figure 7B). Note that this NaCl concentration was chosen because it allowed us to obtain the binding isotherms in a wide range of BSA concentrations, as 20 mM NaCl does not precipitate the AuNPs entirely at low BSA concentrations. The data is fitted to the Hill equation for ligand-receptor interactions (solid red line)[14] to extract the dissociation constant K_D and the Hill coefficient n, which measure the affinity and cooperativity of the interaction, respectively. K_D decreases about twenty times from 600 μM to 30 μM when the NaCl concentration is increased from 0 mM to 20 mM. BSA adsorption reaches monolayer saturation at a BSA concentration < 100 μM in the presence of 20 mM NaCl, while in the absence of NaCl saturation is reached only after 1000 μM. Also, the Hill coefficient slightly increases from 0.6 to 0.9 in the presence of NaCl, indicating that the interaction becomes less anticooperative. Although the hydrodynamic radius at the highest BSA concentration tested (1.5 mM) in the absence of NaCl could indicate the formation of a protein double layer, we cannot discard protein unfolding upon adsorption.[70] Further experiments beyond the scope of this study are required to investigate the possibility of protein conformational changes at low salt concentrations.

In addition to the adsorption isotherms obtained via scattering correlation spectroscopy, we measured the zeta-potential of the AuNPs solutions in the same range of BSA concentrations. The zeta-potential also suggests an increase in affinity for BSA to citrate-stabilized AuNPs in the presence of NaCl. Figure 7C shows zeta-potential measurements as a function of BSA concentration for citrate-stabilized AuNPs at 0 mM (light blue) and 20

mM (dark blue) NaCl. As discussed earlier, the increase in zeta-potential is indicative of BSA adsorption.[31,60] In agreement with the adsorption isotherms presented in Figures 7A and 7B, in the presence of 20 mM NaCl the zeta-potential reaches saturation at a BSA concentration < 100 μM, whereas in the absence of salt, saturation in the zeta-potential is not observed until at least 1000 μM BSA.

The increase in the affinity between BSA and AuNPs in the presence of NaCl suggests that hydrophobic interactions may rule the mechanism of adsorption of BSA onto citrate-stabilized AuNPs. If BSA was binding via electrostatic interactions to the citrate anions bound to the AuNP surface, the binding affinity would have to decrease in the presence of salts because fewer citrate anions are available at the nanoparticle surface, as they are forming complexes with the metal cations as shown above.[31,57,60,62] Also, if BSA was forming a thiol bond with the AuNP surface,[59,61] the sulfhydryl-blocked form of BSA should not provide the enhanced colloidal stability in saline solutions and should not form a similar monolayer adsorption as found for native BSA. Instead it is most likely that the complexation between the citrate anions and the metal cations increases the hydrophobicity of the AuNPs, as the 'naked' AuNP surface becomes increasingly exposed with increasing salt concentration.[12] Using a quartz crystal microbalance Brewer et al. indeed showed a larger preference for BSA to bind to a bare gold surface compared to a citrate-coated gold surfaces.[57] While it is possible that some citrate molecules are still left bound to the AuNP surface and BSA forms a monolayer on top of citrate molecules, the overall increase in hydrophobicity shifts the equilibrium between BSA and AuNPs toward higher binding affinities.

Our results are in good agreement with recent reports. Murphy and co-workers observed that fetal bovine serum enhanced the stability of CTAB coated gold nanorods in the presence of cell culture media.[71] Cedervall et al. suggested that hydrophobic interactions tend to dominate the energy balance between plasma proteins and nanoparticles.[12] In addition, an enhanced stability of BSA-coated AuNPs in simulated intestinal fluid,[72] and negligible hemolytic activity and cytotoxic responses of BSA-stabilized AuNPs in the presence of red blood cells have been reported.[73] It should also be noted that even though the experiments presented here were performed at room temperature, the conformation of the protein is expected to be not affected by this because the denaturation temperature of BSA is at least 18 degrees higher than the physiological temperature.[30] The diffusion coefficients of both BSA and AuNPs are however expected to equally increase under *in vivo* conditions as a result of a higher temperature.

Conclusions

In conclusion, we have shown that citrate-stabilized AuNPs aggregate and precipitate in aqueous solutions with the same NaCl concentration as human blood plasma and commonly used saline buffers. This salt-induced aggregation likely occurs due to the ability of citrate to form complexes with counter ions in solution, leaving the AuNP surface unprotected from Van der Waals interparticle attraction. Adsorption of BSA onto the nanoparticle surface enhances the stability of the colloidal solution to a degree, where monodisperse nanoparticle solutions are stable at NaCl concentrations above the isotonic point (> 100 mM) and similar to commonly used saline buffers and seawater. In addition, we demonstrated that the ionic strength of the solution plays a key role in the formation of the BSA-corona with citrate-stabilized AuNPs. The binding affinity between BSA and AuNPs increases in the presence of salts, likely due to the complexation of the citrate anions with salt cations in solution, thereby increasing the hydrophobicity of the nanoparticle surface. Although the effect of the nanoparticle size was not addressed here, it will likely play a role as we expect that for larger AuNPs a higher relative salt concentration is needed to induce colloidal

aggregation.[74] In addition, the AuNP size could affect the protein adsorption as recent reports suggest an effect of the nanoparticle curvature on the conformation of adsorbed proteins.[33,60]

Our study confirms the role of BSA as the multifunctional transporter of non-polar compounds in environments with high ionic strength such as blood plasma, highlights a positive effect of the BSA protein-corona in the transport of nanoparticles across the bloodstream, and provides a bio-compatible and low-cost strategy for nanoparticle protection in highly ionic environments. In principle, the protection against colloidal aggregation offered by BSA could find use in other nanoparticle-based technologies such as the recently developed nanoparticle steam generation process using sunlight,[75] which could be used for the desalination of sea water if colloidal aggregation under very high salt concentrations can be minimized or ideally completely avoided.

Supplementary Material

Refer to Web version on PubMed Central for supplementary material.

Acknowledgments

S.L. acknowledges support from the Robert A. Welch Foundation [Grant C-1664], the Cancer Prevention and Research Institute of Texas [CPRIT RP110355], and a ARO MURI [W911NF-12-1-0407]. C.F.L. thanks the Robert A. Welch Foundation [Grant C-1787], the National Science Foundation [Grants CBET-1134417 and CHE-1151647], and the National Institutes of Health [Grant GM94246-01A1]. JO acknowledges support from the National Science Foundation through a Graduate Research Fellowship [0940902]. We thank Dr. Wei-Shun Chang for insightful discussions.

References

1. Anderson NL, Anderson NG. The human plasma proteome: history, character, and diagnostic prospects. Mol Cell Proteomics. 2002; 1:845–867. [PubMed: 12488461]
2. Schallen, JGS.; Kampfer, U.; Lejon, S.; Trachsel, C. Human Blood Plasma Proteins. 1. John Wiley & Sons Ltd; West Sussex, England: 2008.
3. Davis ME, Chen Z, Shin DM. Nanoparticle therapeutics: an emerging treatment modality for cancer. Nat Rev Drug Discov. 2008; 7:771–782. [PubMed: 18758474]
4. Chakravarthy KV, Bonoiu AC, Davis WG, Ranjan P, Ding H, Hu R, Bowzard JB, Bergey EJ, Katz JM, Knight PR, Sambhara S, Prasad PN. Gold nanorod delivery of an ssRNA immune activator inhibits pandemic H1N1 influenza viral replication. Proc Natl Acad Sci USA. 2010; 107:10172–10177. [PubMed: 20498074]
5. Kang B, Mackey MA, El-Sayed MA. Nuclear Targeting of Gold Nanoparticles in Cancer Cells Induces DNA Damage, Causing Cytokinesis Arrest and Apoptosis. J Am Chem Soc. 2010; 132:1517–1519. [PubMed: 20085324]
6. Huschka R, Zuloaga J, Knight MW, Brown LV, Nordlander P, Halas NJ. Light-Induced Release of DNA from Gold Nanoparticles: Nanoshells and Nanorods. J Am Chem Soc. 2011; 133:12247–12255. [PubMed: 21736347]
7. Dreaden EC, Alkilany AM, Huang X, Murphy CJ, El-Sayed MA. The golden age: Gold nanoparticles for biomedicine. Chem Soc Rev. 2012; 41:2740–2779. [PubMed: 22109657]
8. Petosa AR, Jaisi DP, Quevedo IR, Elimelech M, Tufenkji N. Aggregation and Deposition of Engineered Nanomaterials in Aquatic Environments: Role of Physicochemical Interactions. Environ Sci Technol. 2010; 44:6532–6549. [PubMed: 20687602]
9. Cho EC, Zhang Q, Xia Y. The effect of sedimentation and diffusion on cellular uptake of gold nanoparticles. Nat Nanotechnol. 2011; 6:385–391. [PubMed: 21516092]
10. Alkilany AM, Murphy CJ. Toxicity and cellular uptake of gold nanoparticles: what we have learned so far? J Nanopart Res. 2010; 12:2313–2333. [PubMed: 21170131]

11. Albanese A, Chan WCW. Effect of Gold Nanoparticle Aggregation on Cell Uptake and Toxicity. ACS Nano. 2011; 5:5478–5489. [PubMed: 21692495]
12. Cedervall T, Lynch I, Lindman S, Berggard T, Thulin E, Nilsson H, Dawson KA, Linse S. Understanding the nanoparticle-protein corona using methods to quantify exchange rates and affinities of proteins for nanoparticles. Proc Natl Acad Sci USA. 2007; 104:2050–2055. [PubMed: 17267609]
13. Dobrovolskaia MA, Patri AK, Zheng J, Clogston JD, Ayub N, Aggarwal P, Neun BW, Hall JB, McNeil SE. Interaction of colloidal gold nanoparticles with human blood: Effects on particle size and analysis of plasma protein binding profiles. Nanomedicine. 2009; 5:106–117. [PubMed: 19071065]
14. Rocker C, Potzl M, Zhang F, Parak WJ, Nienhaus GU. A quantitative fluorescence study of protein monolayer formation on colloidal nanoparticles. Nat Nanotechnol. 2009; 4:577–580. [PubMed: 19734930]
15. Mahmoudi M, Lynch I, Ejtehadi MR, Monopoli MP, Bombelli FB, Laurent S. Protein-nanoparticle interactions: Opportunities and challenges. Chem Rev. 2011; 111:5610–5637. [PubMed: 21688848]
16. Tenzer S, Docter D, Rosfa S, Wlodarski A, Kuharev J, Rekik A, Knauer SK, Bantz C, Nawroth T, Bier C, Sirirattanapan J, Mann W, Treuel L, Zellner R, Maskos M, Schild H, Stauber RH. Nanoparticle size is a critical physicochemical determinant of the human blood plasma corona: A comprehensive quantitative proteomic analysis. ACS Nano. 2011; 5:7155–7167. [PubMed: 21866933]
17. Walkey CD, Chan WCW. Understanding and controlling the interaction of nanomaterials with proteins in a physiological environment. Chem Soc Rev. 2012; 41:2780–2799. [PubMed: 22086677]
18. Dutta D, Sundaram SK, Teeguarden JG, Riley BJ, Fifield LS, Jacobs JM, Addleman SR, Kaysen GA, Moudgil BM, Weber TJ. Adsorbed proteins influence the biological activity and molecular targeting of nanomaterials. Toxicol Sci. 2007; 100:303–315. [PubMed: 17709331]
19. Monopoli MP, Walczyk D, Campbell A, Elia G, Lynch I, Baldelli Bombelli F, Dawson KA. Physical-chemical aspects of protein corona: relevance to in vitro and in vivo biological impacts of nanoparticles. J Am Chem Soc. 2011; 133:2525–2534. [PubMed: 21288025]
20. Walkey CD, Olsen JB, Guo H, Emili A, Chan WCW. Nanoparticle Size and Surface Chemistry Determine Serum Protein Adsorption and Macrophage Uptake. J Am Chem Soc. 2012; 134:2139–2147. [PubMed: 22191645]
21. Salvati A, Pitek AS, Monopoli MP, Prapainop K, Bombelli FB, Hristov DR, Kelly PM, Åberg C, Mahon E, Dawson KA. Transferrin-functionalized nanoparticles lose their targeting capabilities when a biomolecule corona adsorbs on the surface. Nat Nanotechnol. 2013; 8:137–143. [PubMed: 23334168]
22. Doorley GW, Payne CK. Cellular binding of nanoparticles in the presence of serum proteins. Chem Commun. 2011; 47:466–468.
23. Wang B, Zhang L, Bae SC, Granick S. Nanoparticle-induced surface reconstruction of phospholipid membranes. Proc Natl Acad Sci USA. 2008; 105:18171–18175. [PubMed: 19011086]
24. Sabuncu AC, Grubbs J, Qian S, Abdel-Fattah TM, Stacey MW, Beskok A. Probing nanoparticle interactions in cell culture media. Colloids Surf B. 2012; 95:96–102.
25. Jia HY, Liu Y, Zhang XJ, Han L, Du LB, Tian Q, Xu YC. Potential Oxidative Stress of Gold Nanoparticles by Induced-NO Releasing in Serum. J Am Chem Soc. 2008; 131:40–41. [PubMed: 19072650]
26. Nel AE, Madler L, Velegol D, Xia T, Hoek EMV, Somasundaran P, Klaessig F, Castranova V, Thompson M. Understanding biophysicochemical interactions at the nano-bio interface. Nat Mater. 2009; 8:543–557. [PubMed: 19525947]
27. Clift MJD, Bhattacharjee S, Brown DM, Stone V. The effects of serum on the toxicity of manufactured nanoparticles. Toxicol Lett. 2010; 198:358–365. [PubMed: 20705123]

28. Maiorano G, Sabella S, Sorce B, Brunetti V, Malvindi MA, Cingolani R, Pompa PP. Effects of cell culture media on the dynamic formation of protein-nanoparticle complexes and influence on the cellular response. ACS Nano. 2010; 4:7481–7491. [PubMed: 21082814]
29. He XM, Carter DC. Atomic structure and chemistry of human serum albumin. Nature. 1992; 358:209–215. [PubMed: 1630489]
30. Peters, T, Jr. All about Albumin: Biochemistry, Genetics and Medical Applications. 1. Academic Press, Inc; San Diego, Ca: 1996.
31. Casals E, Pfaller T, Duschl A, Oostingh GJ, Puntes V. Time evolution of the nanoparticle protein corona. ACS Nano. 2010; 4:3623–3632. [PubMed: 20553005]
32. Lacerda SHDP, Park JJ, Meuse C, Pristinski D, Becker ML, Karim A, Douglas JF. Interaction of gold nanoparticles with common human blood proteins. ACS Nano. 2010; 4:365–379. [PubMed: 20020753]
33. Deng ZJ, Liang M, Toth I, Monteiro MJ, Minchin RF. Molecular Interaction of Poly(acrylic acid) Gold Nanoparticles with Human Fibrinogen. ACS Nano. 2012; 6:8962–8969. [PubMed: 22998416]
34. Link S, El-Sayed MA. Shape and size dependence of radiative, non-radiative and photothermal properties of gold nanocrystals. Int Rev Phys Chem. 2000; 19:409–453.
35. Willets KA, Van Duyne RP. Localized Surface Plasmon Resonance Spectroscopy and Sensing. Annu Rev Phys Chem. 2007; 58:267–297. [PubMed: 17067281]
36. Tcherniak A, Ha JW, Dominguez-Medina S, Slaughter LS, Link S. Probing a century old prediction one plasmonic particle at a time. Nano Lett. 2010; 10:1398–1404. [PubMed: 20196552]
37. Chang WS, Willingham B, Slaughter LS, Dominguez-Medina S, Swanglap P, Link S. Radiative and Nonradiative Properties of Single Plasmonic Nanoparticles and Their Assemblies. Acc Chem Res. 2012; 45:1936–1945. [PubMed: 22512668]
38. Halas NJ. Plasmonics: An Emerging Field Fostered by Nano Letters. Nano Lett. 2010; 10:3816–3822. [PubMed: 20853888]
39. Haes AJ, Van Duyne RP. A Nanoscale Optical Biosensor: Sensitivity and Selectivity of an Approach Based on the Localized Surface Plasmon Resonance Spectroscopy of Triangular Silver Nanoparticles. J Am Chem Soc. 2002; 124:10596–10604. [PubMed: 12197762]
40. Lasne D, Blab GA, Berciaud S, Heine M, Groc L, Choquet D, Cognet L, Lounis B. Single Nanoparticle Photothermal Tracking (SNaPT) of 5-nm Gold Beads in Live Cells. Biophys J. 2006; 91:4598–4604. [PubMed: 16997874]
41. Lal S, Link S, Halas NJ. Nano-optics from sensing to waveguiding. Nature Photon. 2007; 1:641–648.
42. Chien C-C, Chen H-H, Lai S-F, Hwu Y, Petibois C, Yang CS, Chu Y, Margaritondo G. X-ray imaging of tumor growth in live mice by detecting gold-nanoparticle-loaded cells. Sci Rep. 2012:2.
43. Ament I, Prasad J, Henkel A, Schmachtel S, Sönnichsen C. Single Unlabeled Protein Detection on Individual Plasmonic Nanoparticles. Nano Lett. 2012; 12:1092–1095. [PubMed: 22268768]
44. Zijlstra P, Paulo PMR, Orrit M. Optical detection of single non-absorbing molecules using the surface plasmon resonance of a gold nanorod. Nat Nanotechnol. 2012; 7:379–382. [PubMed: 22504707]
45. Connor EE, Mwamuka J, Gole A, Murphy CJ, Wyatt MD. Gold Nanoparticles Are Taken Up by Human Cells but Do Not Cause Acute Cytotoxicity. Small. 2005; 1:325–327. [PubMed: 17193451]
46. Mirkin CA, Letsinger RL, Mucic RC, Storhoff JJ. A DNA-based method for rationally assembling nanoparticles into macroscopic materials. Nature. 1996; 382:607–609. [PubMed: 8757129]
47. Love JC, Estroff LA, Kriebel JK, Nuzzo RG, Whitesides GM. Self-assembled monolayers of thiolates on metals as a form of nanotechnology. Chem Rev. 2005; 105:1103–1170. [PubMed: 15826011]
48. Wijaya A, Hamad-Schifferli K. Ligand Customization and DNA Functionalization of Gold Nanorods via Round-Trip Phase Transfer Ligand Exchange. Langmuir. 2008; 24:9966–9969. [PubMed: 18717601]

49. Murphy CJ, Thompson LB, Alkilany AM, Sisco PN, Boulos SP, Sivapalan ST, Yang JA, Chernak DJ, Huang J. The Many Faces of Gold Nanorods. J Phys Chem Lett. 2010; 1:2867–2875.
50. Dong A, Ye X, Chen J, Kang Y, Gordon T, Kikkawa JM, Murray CB. A Generalized Ligand-Exchange Strategy Enabling Sequential Surface Functionalization of Colloidal Nanocrystals. J Am Chem Soc. 2011; 133:998–1006. [PubMed: 21175183]
51. Stobiecka M, Deeb J, Hepel M. Ligand exchange effects in gold nanoparticle assembly induced by oxidative stress biomarkers: Homocysteine and cysteine. Biophys Chem. 2010; 146:98–107. [PubMed: 19944518]
52. Zhang X, Servos MR, Liu J. Instantaneous and Quantitative Functionalization of Gold Nanoparticles with Thiolated DNA Using a pH-Assisted and Surfactant-Free Route. J Am Chem Soc. 2012; 134:7266–7269. [PubMed: 22506486]
53. Jana NR, Gearheart L, Murphy CJ. Seeding Growth for Size Control of 5–40 nm Diameter Gold Nanoparticles. Langmuir. 2001; 17:6782–6786.
54. Jana NR, Gearheart L, Murphy CJ. Seed-Mediated Growth Approach for Shape-Controlled Synthesis of Spheroidal and Rod-like Gold Nanoparticles Using a Surfactant Template. Adv Mater. 2001; 13:1389–1393.
55. Nikoobakht B, El-Sayed MA. Preparation and Growth Mechanism of Gold Nanorods (NRs) Using Seed-Mediated Growth Method. Chem Mater. 2003; 15:1957–1962.
56. Zhang X, Servos MR, Liu J. Surface Science of DNA Adsorption onto Citrate-Capped Gold Nanoparticles. Langmuir. 2012; 28:3896–3902. [PubMed: 22272583]
57. Brewer SH, Glomm WR, Johnson MC, Knag MK, Franzen S. Probing BSA binding to citrate-coated gold nanoparticles and surfaces. Langmuir. 2005; 21:9303–9307. [PubMed: 16171365]
58. Chakraborty S, Joshi P, Shanker V, Ansari ZA, Singh SP, Chakrabarti P. Contrasting effect of gold nanoparticles and nanorods with different surface modifications on the structure and activity of bovine serum albumin. Langmuir. 2011; 27:7722–7731. [PubMed: 21591651]
59. Tsai DH, DelRio FW, Keene AM, Tyner KM, MacCuspie RI, Cho TJ, Zachariah MR, Hackley VA. Adsorption and conformation of serum albumin protein on gold nanoparticles investigated using dimensional measurements and in situ spectroscopic methods. Langmuir. 2011; 27:2464–2477.
60. Goy-López S, Juárez J, Alatorre-Meda M, Casals E, Puntes VF, Taboada P, Mosquera V. Physicochemical Characteristics of Protein–NP Bioconjugates: The Role of Particle Curvature and Solution Conditions on Human Serum Albumin Conformation and Fibrillogenesis Inhibition. Langmuir. 2012; 28:9113–9126. [PubMed: 22439664]
61. Sen T, Mandal S, Haldar S, Chattopadhyay K, Patra A. Interaction of Gold Nanoparticle with Human Serum Albumin (HSA) Protein Using Surface Energy Transfer. J Phys Chem C. 2011; 115:24037–24044.
62. Cañaveras F, Madueño R, Sevilla JM, Blázquez M, Pineda T. Role of the Functionalization of the Gold Nanoparticle Surface on the Formation of Bioconjugates with Human Serum Albumin. J Phys Chem C. 2012; 116:10430–10437.
63. Shang L, Wang Y, Jiang J, Dong S. pH-Dependent Protein Conformational Changes in Albumin: Gold Nanoparticle Bioconjugates: A Spectroscopic Study. Langmuir. 2007; 23:2714–2721. [PubMed: 17249699]
64. Ellman GL. Tissue sulfhydryl groups. Arch Biochem Biophys. 1959; 82:70–77. [PubMed: 13650640]
65. Tcherniak A, Dominguez-Medina S, Chang WS, Swanglap P, Slaughter LS, Landes CF, Link S. One-photon plasmon luminescence and its application to correlation spectroscopy as a probe for rotational and translational dynamics of gold nanorods. J Phys Chem C. 2011; 115:15938–15949.
66. Aragon SR, Pecora R. Fluorescence correlation spectroscopy as a probe of molecular dynamics. J Chem Phys. 1976; 64:1791–1803.
67. Tcherniak A, Reznik C, Link S, Landes CF. Fluorescence correlation spectroscopy: Criteria for analysis in complex systems. Anal Chem. 2008; 81:746–754. [PubMed: 19093758]
68. Francis AJ, Dodge CJ, Gillow JB. Biodegradation of metal citrate complexes and implications for toxic-metal mobility. Nature. 1992; 356:140–142.

69. Dominguez-Medina S, McDonough S, Swanglap P, Landes CF, Link S. In Situ Measurement of Bovine Serum Albumin Interaction with Gold Nanospheres. Langmuir. 2012; 28:9131–9139. [PubMed: 22515552]

70. Pan H, Qin M, Meng W, Cao Y, Wang W. How Do Proteins Unfold upon Adsorption on Nanoparticle Surfaces? Langmuir. 2012; 28:12779–12787. [PubMed: 22913793]

71. Alkilany AM, Nagaria PK, Hexel CR, Shaw TJ, Murphy CJ, Wyatt MD. Cellular Uptake and Cytotoxicity of Gold Nanorods: Molecular Origin of Cytotoxicity and Surface Effects. Small. 2009; 5:701–708. [PubMed: 19226599]

72. Fang R, Hao R, Wu X, Li Q, Leng X, Jing H. Bovine Serum Albumin Nanoparticle Promotes the Stability of Quercetin in Simulated Intestinal Fluid. J Agric Food Chem. 2011; 59:6292–6298. [PubMed: 21542648]

73. Khullar P, Singh V, Mahal A, Dave PN, Thakur S, Kaur G, Singh J, Singh Kamboj S, Singh Bakshi M. Bovine Serum Albumin Bioconjugated Gold Nanoparticles: Synthesis, Hemolysis, and Cytotoxicity toward Cancer Cell Lines. J Phys Chem C. 2012; 116:8834–8843.

74. Li X, Lenhart JJ, Walker HW. Aggregation Kinetics and Dissolution of Coated Silver Nanoparticles. Langmuir. 2012; 28:1095–1104. [PubMed: 22149007]

75. Neumann O, Urban AS, Day J, Lal S, Nordlander P, Halas NJ. Solar vapor generation enabled by nanoparticles. ACS Nano. 2013; 7:42–49. [PubMed: 23157159]

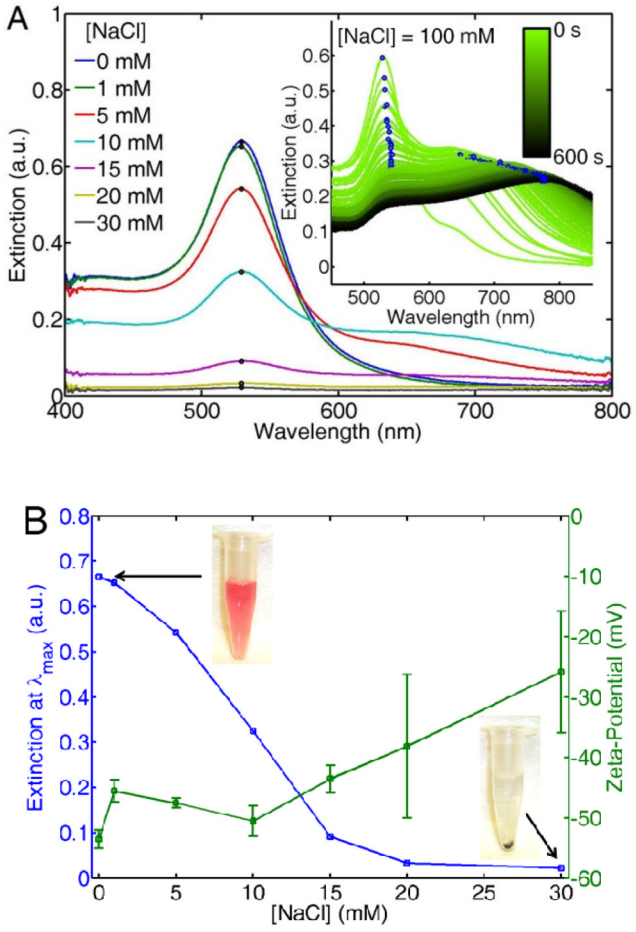

Figure 1.

(A) UV/Vis extinction spectra of citrate-stabilized AuNPs for increasing NaCl concentrations after 24 hours of storage at room temperature. The inset shows extinction spectra as a function of time for the first 600 s of the precipitation process. (B) Extinction at λ_{max} as a function of NaCl concentration extracted from equilibrated spectra in (A), along with zeta-potential measurements of the same NP solutions. Pictures of two representative solutions are shown as insets. The error bars are calculated from the peak value of the zeta-potential acquired from three independent measurements.

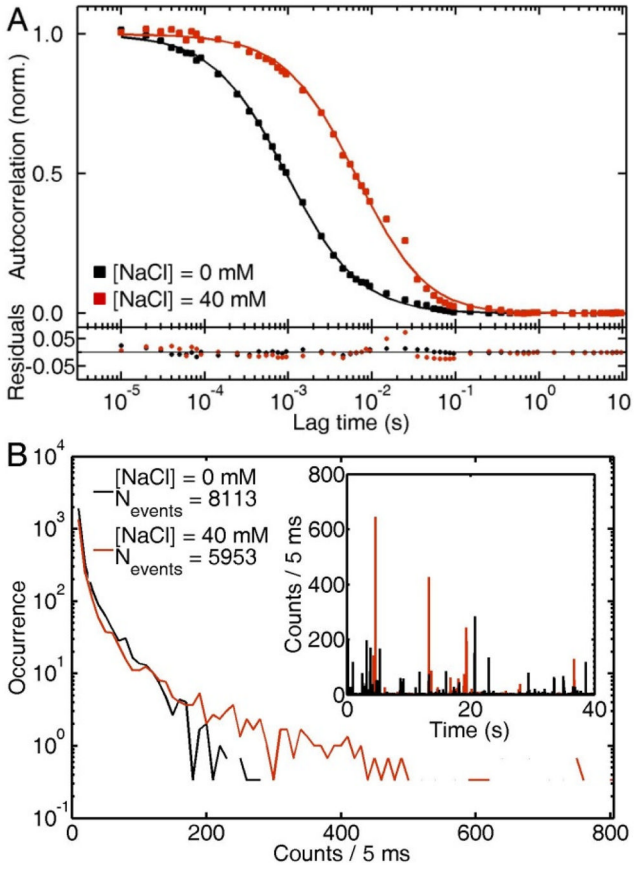

Figure 2.

(A) Autocorrelation traces of citrate-stabilized AuNPs in water (black) and after addition of 40 mM of NaCl (red). (B) Blip intensity frequency analysis (BIFA) extracted from the same raw intensity traces (inset) used in the autocorrelation anaysis presented in (A).

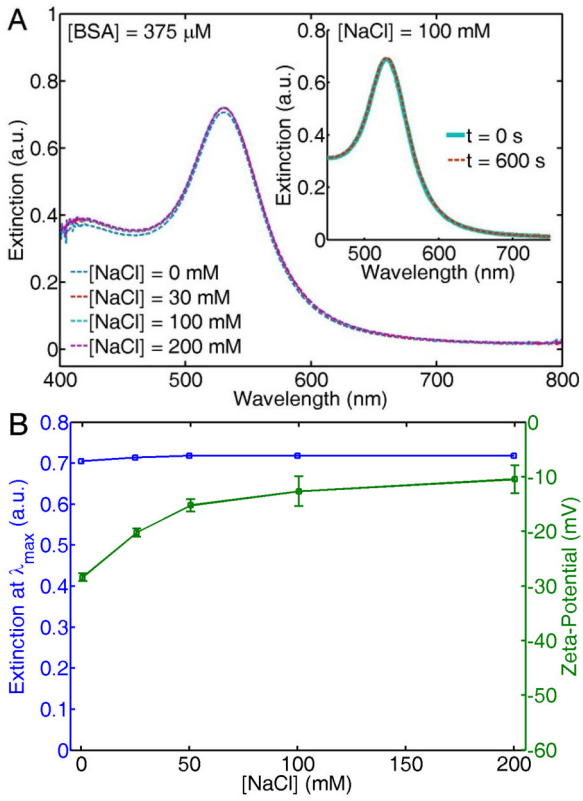

Figure 3.

(A) UV/Vis extinction spectra of citrate-stabilized AuNPs mixed with BSA (375 μM) before addition of increasing NaCl concentrations, measured after 24 hours of storage at room temperature. The inset shows the extinction spectra of AuNPs after simultaneous addition of BSA (375 μM) and NaCl (100 mM) at t = 0 s (solid-cyan line) and at t = 600 s (dashed-red line). (B) Extinction at λ_{max} as a function of NaCl concentration extracted from the spectra in (A), along with zeta-potential measurements of the same solutions.

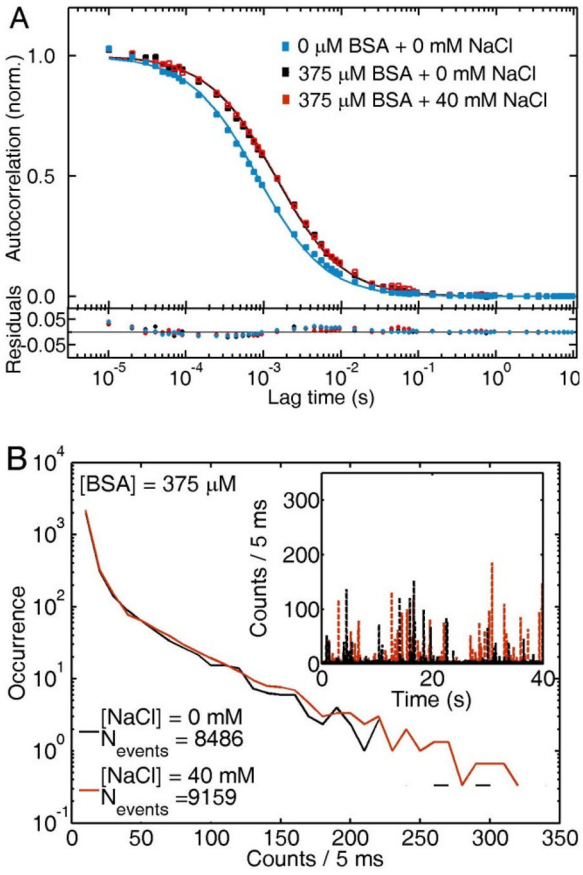

Figure 4.

(A) Autocorrelation curves of citrate-stabilized AuNPs (blue squares), and BSA-bound AuNPs in 0 mM (black squares) and 40 mM NaCl (red squares) solutions. (B) Blip intensity frequency analysis (BIFA) extracted from the same intensity traces (inset) used in the autocorrelation analysis presented in (A).

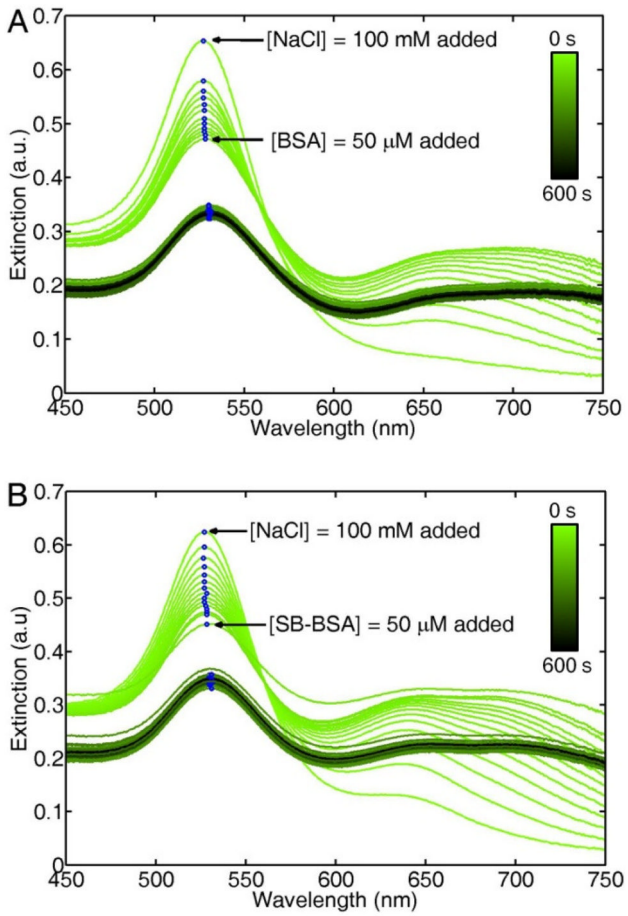

Figure 5.

(A) UV/Vis extinction spectra of citrate-stabilized AuNPs as a function of time after addition 100 mM NaCl. 50 μM BSA is added at t = 10 s. (B) Same experiment as presented in (A), except that a sulfhydryl-blocked form of BSA (SB-BSA) is added at t = 10 s. The blue dots highlight the maximum extinction of each spectrum. The drop in extinction after BSA addition is due to dilution of the AuNP solution.

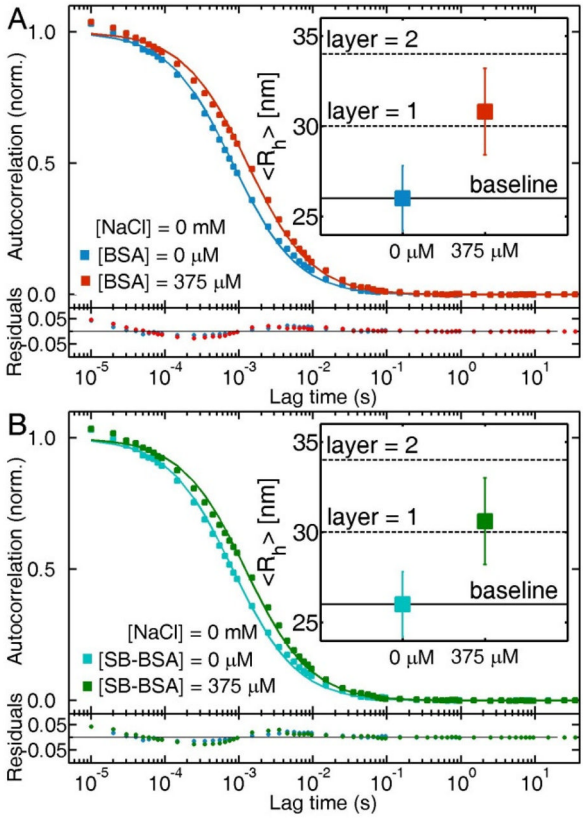

Figure 6.

Autocorrelation traces of citrate-stabilized AuNPs before and after addition of BSA (A) and SB-BSA (B) at physiological concentrations (375 μM). The insets contain the calculated in hydrodynamic radius of the AuNPs based on the measured characteristic diffusion times.

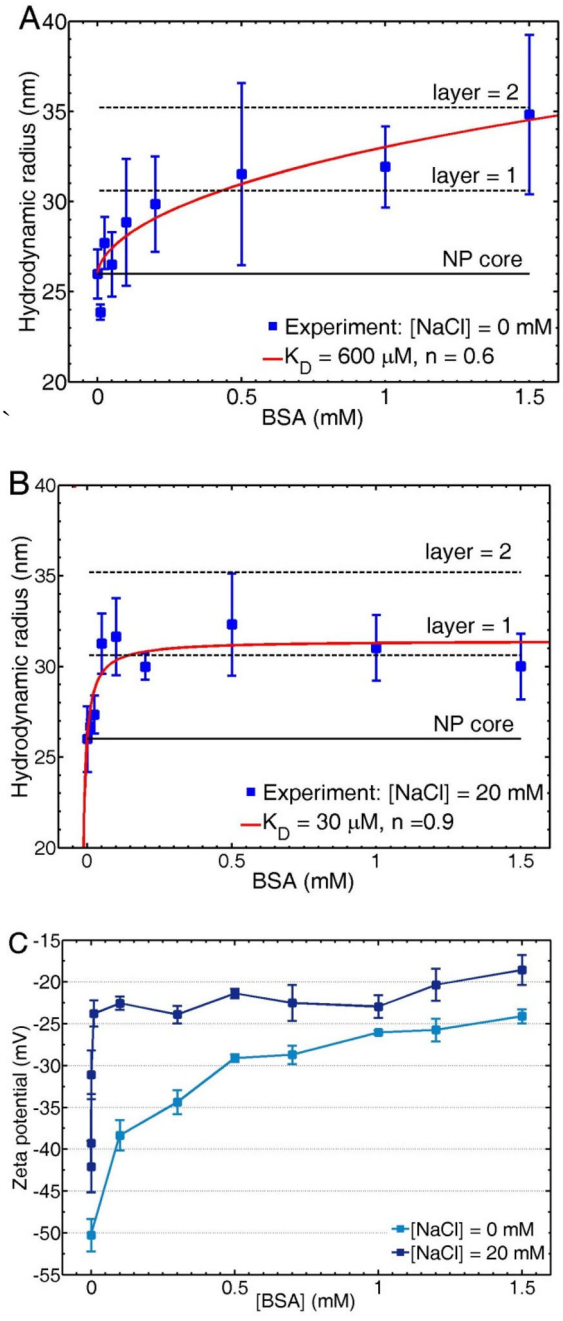

Figure 7.

Adsorption isotherms of BSA onto citrate-stabilized AuNPs in 0 mM (A) and 20 mM NaCl (B). The experimental data points obtained via scattering correlation spectroscopy (blue squares) are fitted to the Hill equation (red line). The NP core (R_h = 26 nm) and theoretical protein layers ($\Delta R_h \approx 4$ nm) are shown as eye guides. (C) Zeta-potential experiments of citrate-stabilized AuNPs as a function of BSA concentration in the presence of 0 mM and 20 mM NaCl. Error bars show the standard deviation calculated out of at least three independent measurements.